ADVANCED MATERIALS INTERFACES
www.advmatinterfaces.de

Polymer-Stabilized Monodomain Blue Phase Diffraction Grating

Ramesh Manda, Srinivas Pagidi, Yun Jin Heo, Young Jin Lim, Min Su Kim, and Seung Hee Lee**

The structural beauty of liquid crystalline blue phases is attested not only by their colorful optical micrographic textures but also by optical isotropy. More importantly, the homogeneity of the structures influences greatly to the electro-optic properties. In this work, how the lattice orientation in polymer-stabilized blue phase liquid crystal (PS-BPLC) diffraction grating affects phase-modulated diffraction efficiency is elaborated. A well-arranged monodomain structure of blue phase is achieved and its diffraction capability is compared with multidomain PS-BPLC. The diffraction efficiency in the zeroth order of monodomain PS-BPLC is improved by 9% compared to that of multidomain structure. In addition, both driving and threshold voltages in monodomain PS-BPLC are decreased by 29% and 30%, respectively, compared to those in multidomain PS-BPLC owing to the regular arrangement of cubic lattices that give rise to increase in the coherence length and unified response in molecular reorientation under electric fields. Furthermore, the monodomain PS-BPLC shows an efficient polarization conversion of linear polarization into circular polarization. It is believed that the device exhibits great potential to be used as a polarization converter or beam steering devices.

1. Introduction

Photonic devices give rise to useful elements in laboratory and industries when they become more portable and compact. Removing parts for mechanical motion and enhancing switching time in the devices also guarantee the improvement of the photonic devices. From this perspective, liquid crystal (LC) materials can be used as a next-generation photonic application, in particular, when it shows blue phase liquid crystals (BPLCs) because of their unique structural property and fluid-like crystalline structures.[1–5] BPLC has been found to be a prominent material owing to their optical isotropy from cubic symmetry. Although the internal structure of BP is quite complicated, they are self-assembled in a thermodynamically spontaneous way when chirality is about several hundreds of nanometers. LC directors are doubly twisted at this high chirality and self-assembled into a double-twisted cylinder (DTC). The way that the DTCs are stacked determines the symmetry of the BPLC structure, and the lattice length scale in common includes the visible wavelength, which appears as colorful micrographic textures. From an application perspective, a remarkable breakthrough is that polymer-stabilization method is able to extend their narrow temperature range.[6] Dispersion of nanoparticles (organic/inorganic colloids and perovskite quantum dots) or bent-core LCs and 3D confinement of BPLC like microencapsulation is also reported that it can extend the temperature range of BPs.[7–10] The polymer-stabilized BPLC (PS-BPLC) by in situ photopolymerization is a promising method not only for extending the BP temperature range but also for enhancing their electro-optic performance, such as optical isotropy,[11] selective reflection,[12] less hysteresis,[13] and fast response time.[14] Despite a successful prototyping into a PS-BPLC display,[4] the PS-BPLC has rather shown their possibility of applying to versatile photonic applications such as a diffraction grating,[15] vortex beam generation,[16] optical filters,[17] optical resonators,[18] polarization converter,[19] photonic crystal,[20] and augmented reality/virtual reality.[21]

Up to date, several diffraction grating technologies, such as phase grating and amplitude grating,[22] hybrid grating,[23] one-step holographic grating,[24] and fork grating,[16] have been reported by using BPLC materials because these are advantageous for the non-mechanical beam steering. Such results support that BPLC is one of the promising materials to create such novel functional devices. However, the performance of the device is deteriorated by the multidomain structure of BPLCs. For example, the diffraction efficiency decreases significantly. Despite such importance, less attention has been paid to create and study about monodomain BPLCs for diffraction gratings among several studies previously reported.[16,25–27] Some approaches report that, to resolve the unwanted multiple colors from polycrystalline lattice structure, one can adjust the chiral pitch of BPLCs and have the Bragg wavelength shifted far away from the wavelength of device operation. For instance, when the desired wavelength is within the visible region, one can control the chiral pitch to position the Bragg wavelength within UV region. However, this approach is limited to an

Dr. R. Manda, S. Pagidi, Y. J. Heo, Dr. Y. J. Lim, Prof. S. H. Lee
Applied Materials Institute for BIN Convergence
Department of BIN Convergence Technology and Department of Polymer Nano Science and Technology
Jeonbuk National University
Jeonju, Jeonbuk 54896, Republic of Korea
E-mail: lsh1@jbnu.ac.kr
Dr. M. S. Kim
Department of Physics and Astronomy
Johns Hopkins University
Baltimore, MD 21218, USA
E-mail: mkim182@jhu.edu
The ORCID identification number(s) for the author(s) of this article can be found under https://doi.org/10.1002/admi.201901923.

DOI: 10.1002/admi.201901923

optical aspect. It is required to take into account more detailed electro-optical effect via structural study because the electro-optic response of BPLCs is highly related to their structure. Some basic researches on BPs since 1970s tell us the electro-optic responses are classified depending upon how strongly the electric field is applied to the BPLCs, those are, local reorientation, electrostriction and phase transition.[28] Kim et al. reported that amorphous BP shows a uniform local reorientation of the LC director and much faster electro-optic response whereas the polycrystalline structure of cubic BPs exhibits much disrupted behavior under switching of electric fields.[29] Similarly, a monodomain structure of cubic BPs can enable us to lead to control the reorientation of the LC director in a much homogeneous way. Thus, monodomain structure of BPLCs is prominent for electro-optic and electrophotonic applications as various approaches have been reported from previous works in this field.[30–33] In order for creating a high-performance diffraction grating, it is essential to study the performance of BPLCs with respect to the lattice orientation.

Here, we demonstrate a dynamically controllable diffraction grating based on monodomain PS-BPLCs and elucidate the lattice orientation effect on diffraction efficiency. In previous works, we have demonstrated monodomain BPLCs that exhibit long-range ordered cubic lattices by a meticulous rubbing treatment on a polyimide layer (as likely done in most of commercialized LC displays).[31] By doing so, we are able to create a monodomain BPLC diffraction grating device with guaranteed fabrication consistency. In order to evaluate the performance improvement, we additionally fabricate multidomain BPLC diffraction grating, and then characterize the electro-optic performances, such as the threshold and driving voltages of both mono- and multidomain BPLCs. We use a reactive monomer that exhibits multiple functional groups to be cross-linked. We expect that the PS-BPLC would lead robust stabilization property owing to large cross-linking density after polymerization. This monomer is commercially available so that the reproducibility is still guaranteed for other applications. We also examine how much the linear polarization of an incident light can be converted into other polarization states for each case. This result can show that how the light can efficiently be retarded via the monodomain BPLC structure under an applied electric field. At final, we fabricate a sample by using the same BPLC material and fabrication process but different electrode dimension to know how spatial electric field modulation affects the performance of the proposed BPLC diffraction grating.

2. Theory

It is common that the length of the chiral pitch p in chiral nematic systems is determined as

$$p = \frac{1}{c \cdot \mathrm{HTP}} \tag{1}$$

where HTP and c denote helical twisting power and concentration of the chiral molecules dispersed in nematic LCs. And the p determines the lattice constant a of BPs.[34] The BP is usually classified as BPI, BPII, and BPIII, depending on the symmetry of the lattices. The BPI and BPII exhibit the cubic symmetry whereas the BPIII is amorphous structure. Theoretically, in BPI, $p = a$ whereas $p = a/2$ in BPII. When the incident light is in the range of the visible wavelength that is compatible to a, a wavelength-selective Bragg reflection occurs and it is expressed as[35]

$$\lambda_B = \frac{2n_{avg}a}{\sqrt{h^2 + k^2 + l^2}} \tag{2}$$

where n_{avg} is the average refractive index of the LC ($n_{avg} = (n_e + 2n_o)/3$), and h, k, l are Miller indices. When a sample cell is filled with the BPLC with no surface treatment, multiple colors appear each with its own lattice orientation (**Figure 1**a). However, when a sample cell is filled with the BPLC with a well-treated surface, the orientation of all the lattices is in a particular direction and single color appears (Figure 1b).[30,36]

We outline the working principle of PS-BPLC diffraction grating (Figure 1c,d). At the voltage-off state, there is no spatial

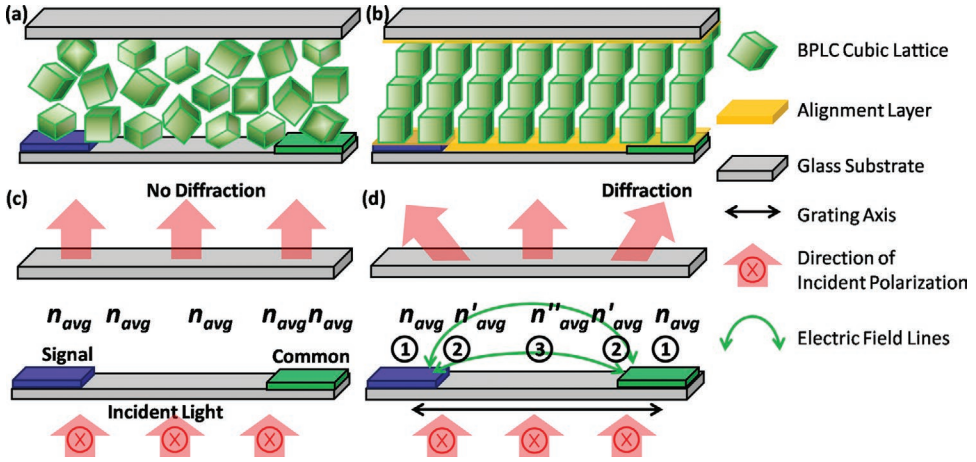

Figure 1. Schematic representation of a) multidomain and b) monodomain BPLC structures and their diffraction at c) voltage-off and d) voltage-on. The green arrows represent simplified electric field lines and the black arrow indicates the direction of linearly polarized light. n_{avg}: average refractive index of BPLC in (c) and region 1 in (d); n'_{avg}: refractive index at electrode edges, region 2 in (d); n''_{avg}: refractive index at the mid-area between electrodes, region 3 in (d).

variation of refractive index owing to the optical isotropy of PS-BPLC (Figure 1c). At the voltage-on state, the electric field induces the local reorientation of LC director. It causes LC birefringence along the electric field between electrodes owing to the Kerr effect, and thus regular, spatial modulation of refractive index takes place (Figure 1d). When a laser beam propagates through the PS-BPLC layer at the voltage-off state, no diffraction occurs as schematically described in Figure 1c. On the other hand, at the voltage-on state, the light experiences the modulated refractive index in the lateral direction with the characteristic length that corresponds to the pitch of the patterned electrodes so that the light is diffracted as shown in Figure 1d.

The diffraction phenomena can be described as[37]

$$n\Lambda \sin\theta = m\lambda \tag{3}$$

where n is the refractive index of the medium, Λ is the grating pitch, θ is the diffraction angle, and m is the diffraction order. At the voltage-on state (Figure 1d), the refractive index in the initial isotropic state n_{avg} is unchanged at region 1 whereas it changes to the field-induced refractive index $n'_{avg}(E)$ at region 2 and $n''_{avg}(E)$ at region 3. At region 2, the LC director tilts along the field direction and it varies along the light propagation direction, and this light propagation direction also changes as the light passes through the z-axis. At region 3, the LC director lies parallel to in-plane field direction so that n_e'' and n_o'' become close to n_e and n_o of the host LC in PS-BPLC. In lateral direction from regions 1 to 3, the refractive index continuously varies from n_{avg} to either $n'_{avg}(E)$ or $n''_{avg}(E)$ in which the linearly polarized light is either parallel or perpendicular to the grating axis. We should note that the notations of spatially resolved refractive index is unable to explicitly describe the system, but it tells us qualitative information about how the light works on the system. Roughly, we can tell the refractive index in each region as $n_e'' > n_e' > n_{avg}$, $n_o'' < n_o' < n_{avg}$, and $|n_{avg} - n_e''| > |n_{avg} - n_o''|$. Thus, we could expect that the diffraction effect with the linearly polarized light, parallel to the grating axis that corresponds to n_e'' is relatively greater than the other polarization mode. When considering polarization, it is also necessary to define the induced birefringence, which is expressed as $\Delta n_{ind}(E) = n_e(E) - n_o(E) = \lambda K E^2$, where K is the Kerr constant and λ is the wavelength of incident light.[38,39] The spatially modulated electric fields contribute to spatial modulation of the induced birefringence. It is useful to know whether the diffraction grating is in Bragg or Raman–Nath regimes.[40] The Klein factor can give a criterion to distinguish two diffraction regimes $Q = \frac{2\pi\lambda_0 d}{n_{avg}\Lambda^2}$, where λ_0 is the wavelength in vacuum, d is the grating thickness, and Λ is grating spacing.

3. Results and Discussion

We observe the sample cell that is filled with a prepared BPLC mixture under a polarized optical microscope (POM) and perform the in situ photopolymerization (see details in the Experimental Section). In order to evaluate BP existing temperature ranges, i.e., its stability after polymer stabilization, we observe textures of both multidomain and monodomain PS-BPLCs under POM where the temperature ramps down from isotropic to nematic phase (**Figure 2**). Figure 2a shows multidomain BPs

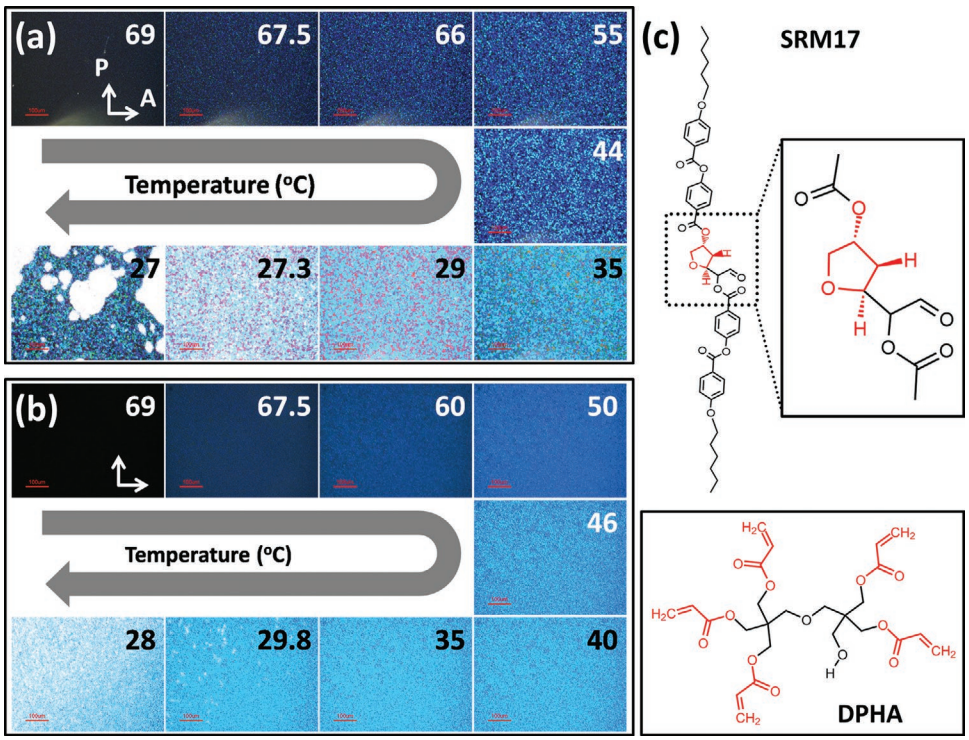

Figure 2. POM textures of a) multidomain and b) monodomain PS-BPLCs. The number in each image indicates temperature (°C). The images were taken while cooling from isotropic phase. c) The molecular structures of chiral dopant SRM17 and monomer DPHA.

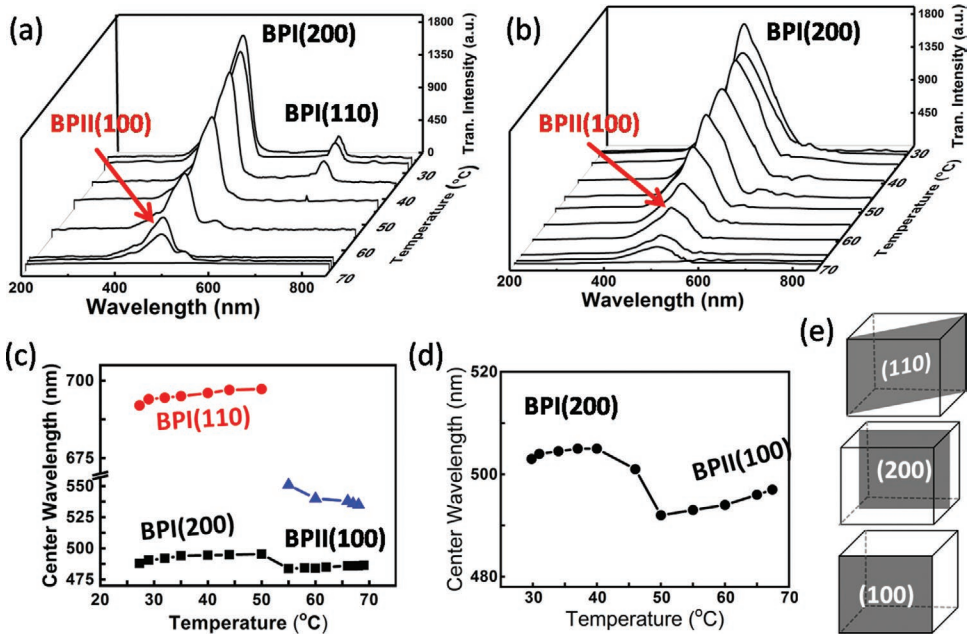

Figure 3. Measured Bragg reflection spectra in, a) multidomain and b) monodomain PS-BPLC with corresponding Miller indices of cubic planes. The temperature-dependent peak wavelength of c) multidomain and d) monodomain PS-BPLC. e) The Miller planes with respect to cubic lattices.

with multiple colored textures in which no surface treatment is done. The multidomain BP is observed over the range of 40.5 °C from 67.8 to 27.3 °C (Iso/67.8 °C/BPII/54.4 °C/BPI/27.3 °C/N*). Figure 2b shows a single colored POM texture of monodomain PS-BPLC on a rubbed polyimide surface. Depending on how the lattices are oriented on the surface, the color appears. The monodomain PS-BPLC shows the Bragg reflection near the bluish region, which is commonly observed in multidomain case. Both BPII and BPI exhibit a monodomain with dark-blue and light-blue colors, respectively. The monodomain BP is observed over the range of 37.6 °C from 67.4 to 29.8 °C (Iso/67.4 °C/BPII/48.2 °C/BPI/29.8 °C/N*). As we expected the stability is sufficiently achieved for application owing to the strong polymer network that imprints the disclinations and reduces the free energy of the system with the reactive monomers, which exhibit multiple functional groups (Figure 2c).

We measure Bragg reflection spectra to identify the observed BPs in details (**Figure 3**). The multidomain PS-BPLC shows sharp multiple reflection peaks (Figure 3a) while the monodomain PS-BPLC exhibits a single reflection peak (Figure 3b). The measured reflection peaks are in a good agreement with the POM textures. The measured reflection peaks in multidomain PS-BPLC appear in both BPI (λ_B = 490 and 695 nm) and BPII (λ_B = 485 nm). We estimate the length of the chiral pitch by using the Equation (1) and the corresponding Miller planes by Equation (2). The calculated chiral pitch length is 317 nm. Thus, we can deduce that the measured reflection peak at 485 nm corresponds to (100) plane in BPII. In BPI, the peaks at 695 and 490 nm correspond to (110) and (200) planes, respectively. In monodomain PS-BPLC, the single peak appears in both BPI (λ_B = 505 nm) and BPII (λ_B = 490 nm), which correspond to (200) and (100) planes, respectively. It is clear that the polyimide-rubbed surface leads to the monodomain BPLC structure. The temperature-dependent measurement of the peak wavelength in multidomain and monodomain PS-BPLC is shown in Figure 3c,d, respectively. The discontinuity in between Bragg reflection peaks implies the phase transition between BPI and BPII. The reflection peaks that shift toward shorter wavelengths could be due to decrease in the chiral pitch as decrease in temperature. The orientation of the Miller planes is schematically shown in Figure 3e.

We measure the diffraction properties of the samples which we estimate the Miller planes at (110), (200) planes for multidomain and (200) plane for monodomain PS-BPLC. We calculate the Klein factor Q = 0.96 and it is in the Raman–Nath (thin) regime. It is also necessary to calculate Fresnel number, defined as $\frac{\Lambda^2}{\lambda R}$, is 3.5×10^{-5} (<<1) that suggests the diffraction is Fraunhofer diffraction, meaning that the diffraction phenomenon is due to far field approximation.

The experimental setup for observation of the diffraction pattern is schematically shown in **Figure 4**a. The diffraction images of mono- and multidomain PS-BPLCs are shown in Figure 4b. The incident laser beam is linearly polarized. The laser beam mostly transmits to the 0th order at 0 V and the slightly higher beam intensity at 1st and 2nd orders is from the patterned electrode (we call this electrode structure as Cell-1 whose electrode width w and spacing l are $w = l = 2$ µm). We choose 40 V for comparison of the diffraction images between mono- and multidomain because the diffraction efficiency is quite saturated at this voltage for both cases (Figure 4c,d). The measured diffraction angle and diffraction efficiency are summarized in **Table 1**. Here, the diffraction angle is estimated from a simple geometrical consideration, $\tan\theta_m = \frac{D_m}{L}$, where the D is the distance between mth and 0th orders and the diffraction space L is the distance between the screen and the sample. The diffraction efficiency is defined as, $\eta_m\,(\%) = \frac{I_m(V)}{I_o} \times 100$, where $I_m(V)$ is

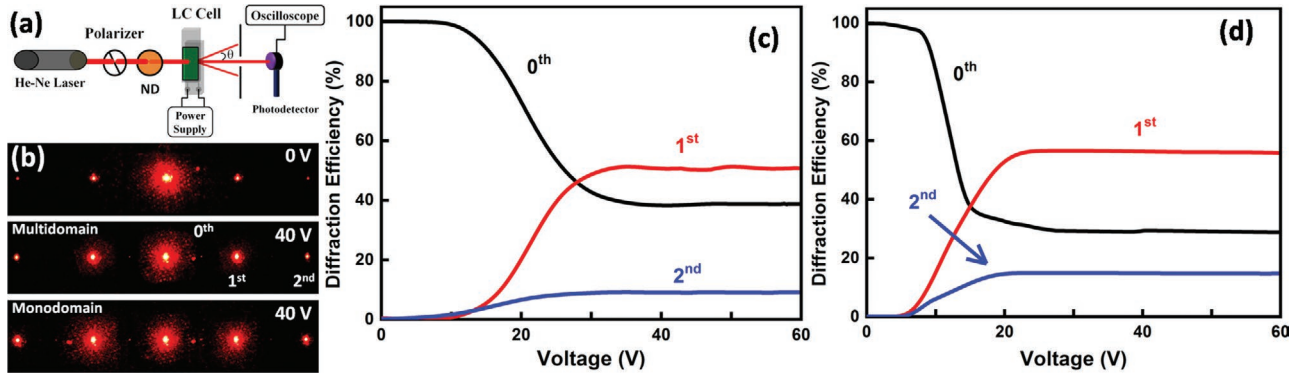

Figure 4. Diffraction measurement of the PS-BPLC. a) The optical setup. ND: neutral density filter. θ: diffraction angle. b) The diffraction pattern from multidomain and monodomain PS-BPLC. The measured diffraction efficiency of c) multidomain and d) monodomain PS-BPLC.

the diffracted light intensity of mth order at voltage V, and I_o is transmitted light intensity of 0th order at voltage-off.

The diffraction angles are unchanged because the patterned electrode spacing is fixed. We also demonstrate the diffraction patterns with narrower diffraction angles in Figures S1 and S2 (Supporting Information), in which the relation between the diffraction angle and grating pitch is governed by Equation (3). In this measurement, the sample is prepared with the consistent condition as Cell-1 but different electrode structure ($w = l = 15$ µm), named as Cell-2.

The voltage-dependent diffraction efficiency curves of the multidomain and monodomain cases are shown in Figure 4c,d. It is clear that the overall diffraction efficiency is higher in monodomain case. The monodomain PS-BPLC exhibits ≈9% and 5.6% increase in 0th and 1st order efficiency, respectively. Here, the 1st order diffraction efficiency refer to resultant effect of both +1st and −1st orders. We believe the enhanced diffraction efficiency of the monodomain PS-BPLC is originated from the higher phase modulation of homogeneously aligned cubic lattice arranged in a similar fashion.[30] It is also interesting to point out that both V_{th} (voltage for 10% transmittance) and V_{op} (voltage for 90% transmittance) are found to be reduced in monodomain BPLC. The monodomain structure more dominantly influences on V_{th} and V_{op} than the surface anchoring caused by the rubbed polyimide surface.

In order to verify the reliability of the performance, we measure the switching behavior (**Figure 5**). We apply a square-wave at 1 kHz to the samples and sweep voltages while observing POM images in which crossed polarizers are diagonally set to the long axis of the patterned electrode. The cells become bright as the voltage applied due to the induced birefringence. As per removing the voltage, the initial texture is completely restructured (Figure 5a,b). We also measure the response time up on the electrical waveform, as shown in Figure 5c,d. The rise times are 0.4 and 0.5 ms whereas the decay times are 2.2 and 2.1 ms for multi and monodomain BPLC, respectively. The rise and decay times are slightly different between the cases. We note that the decay time is relatively slower than the sub-milliseconds decay time previously reported in PS-BPLC system.[6,11] The absence of mesogenic polymer implies that the polymer networks mostly exist at the disclinations. The interfacial area between LC director and polymer networks is relatively less than the case when the mesogenic polymer is entangled within the bulk LC region. Thus, the decay time tends to slightly be slower. We further measure the voltage-dependent retardation. The measured threshold and operation voltages are V_{th} = 13 V, V_{op} = 46 V for multidomain and V_{th} = 9 V, V_{op} = 36 V for monodomain BPLC. The maximum transmittance can be achieved, where $d\Delta n_{ind} = \lambda/2$. The measured retardation is not sufficient condition to $\lambda/2$ in which λ = 582 nm in this measurement because the local reorientation is not fully induced to meet $d\Delta n_{ind}$ = 291 nm. For the comparison of both multi- and monodomain cases, however, the induced retardation of monodomain case at 40 V measures about 13 nm higher than multidomain case (Figure 5e,f). It can contribute to enhance the diffraction efficiency.

Table 1. Diffraction properties of the multidomain and monodomain PS-BPLC, measured at 40 V.

Order	Diffraction angle [°]	Diffraction efficiency [%]	
		Multidomain	Monodomain
1st	2.5	51.1	56.7
2nd	4.8	9.1	14.8

We measure the polarization properties of the multi- and monodomain structures at the 0th (at 0 V) and 1st (40 V) orders. The measurement set in Figure 5c–f is retained for the polarization measurement, except we rotate the analyzer in anticlockwise direction. When the linear polarization of the incident light (the first row of **Figure 6**) experiences the sample at 0 V, it converts to elliptical polarization for multidomain sample whereas it is circularly polarized for the monodomain sample (the second row of Figure 6). At the 1st order when applying 40 V, the linearly polarized light becomes circular polarization for both multi- and monodomain samples, but higher degree of circular polarization with the monodomain sample. We further measure the Stokes parameters to estimate the detailed polarization properties.[41] The Stokes parameters are defined as, $S_0 = I_0 + I_{90}$, $S_1 = I_0 - I_{90}$, $S_2 = I_{45} - I_{-45}$, and $S_3 = I_{RCP} - I_{LCP}$. The calculated values at the 1st order are S_0 = 1.87 (1.7), S_1 = 0 (0.1), S_2 = 0.06 (–0.22), and S_3 = 1.75 (1.68) for monodomain BP (multidomain BP). Here S_3 is defined as $\sqrt{S_0^2+S_1^2+S_2^2}$ and the degree of polarization defined as $\sqrt{S_1^2+S_2^2}/S_o$. The degree of polarization at 0th order (1st order) is 0.18 (0) and 0.26 (0.13) for monodomain and multidomain, respectively. We note that

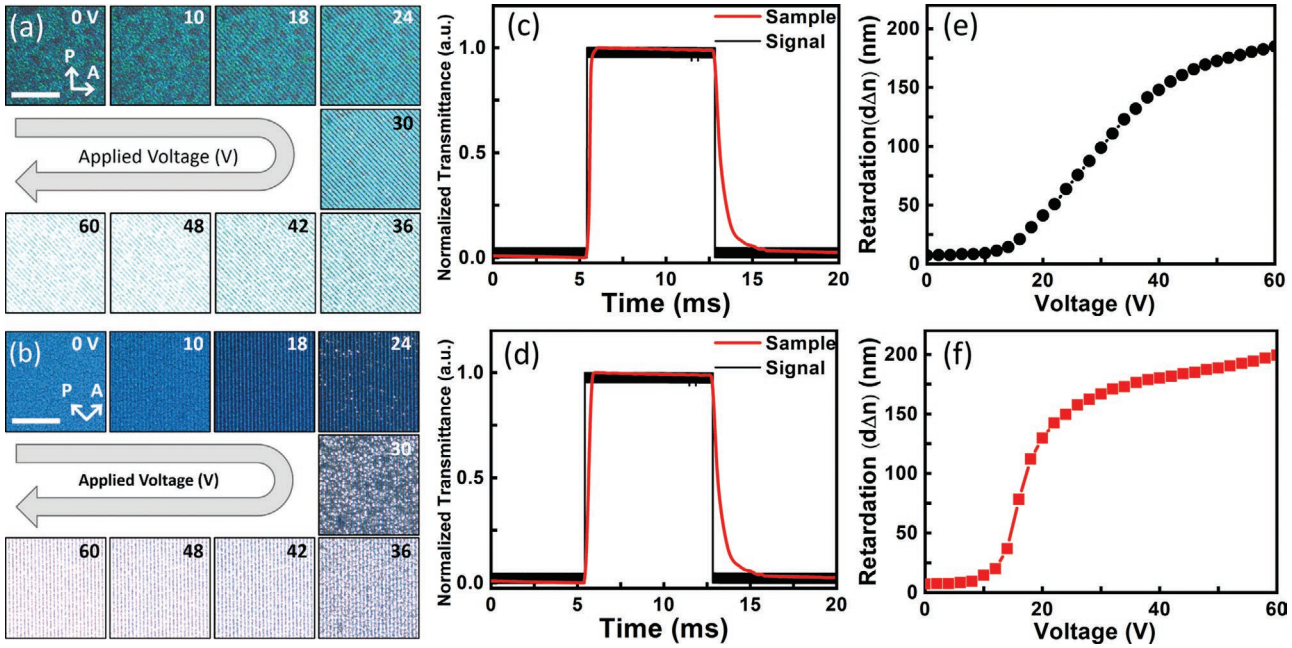

Figure 5. The switching behavior of a,c,e) multidomain PS-BPLC and b,d,f) monodomain PS-BPLC samples under crossed polarizers. a,b) POM images with respect to applied voltages. P and A represent polarizer and analyzer, respectively. c,d) Measured response time. e,f) Measured retardation at $\lambda = 582$ nm.

the polarization state can be controlled by adjusting the applied electric field.

4. Conclusion

The monodomain structure of PS-BPLC is effective on the electro-optic performance of a tunable diffraction grating. We fabricate a monodomain BPLC, the interface of which on the substrate surface is treated by rubbing with a velvet cloth to give regular polymer grooves. The polymer-stabilization technique helps widen the temperature range of monodomain BPLC by mixing the BPLC mixture with a functional monomer. With the monodomain structure, we improve the performance of PS-BPLC diffraction grating. The diffraction efficiency is improved by 9%. The threshold and operating voltages are decreased by 29% and 30%, respectively. In addition, the phase shift of polarized light that experience through the BPLC becomes more complete: the linear polarization is well converted into a circular polarization. The multidomain sample is unable to completely convert the linear polarization into a circular polarization but an elliptical polarization. We believe the proposed monodomain PS-BPLC can be used as high-performance diffraction grating, including a polarization converter or polarimetry devices.

5. Experimental Section

Materials: A BPLC mixture consists of nematic LC (MAT-07-1251, Merck Advanced Technology, Korea; dielectric anisotropy $\Delta\varepsilon = 30.1$ at 1 kHz, birefringence $\Delta n = 0.1492$ at 589.3 nm, clearing temperature $T_{NI} = 68$ °C, rotational viscosity $\gamma_1 = 279$ mPa s), a commercially unavailable laboratory-synthesized chiral dopant (SRM17, helical twisting power (HTP) = 166 μm^{-1}), a photocurable monomer (dipentaerythritol penta/hexa-acrylate (DPHA), Sigma Aldrich, Korea), and a photoinitiator (Irgacure-907, Sigma Aldrich, USA). The molecular structures of SRM17 and DPHA are shown in Figure 2c. The concentration (wt%) of each material in the BPLC mixture is LC/chiral dopant/monomer/photoinitiator (85.1/1.9/12/1).

Sample Cell Preparation: In order to characterize the BPLC mixture, two set of in-plane switching type cells were prepared and named as Cell-1 and Cell-2. Both Cell-1 and Cell-2 contains comb-like interdigitated ITO (indium-tin-oxide) electrodes on the bottom substrate, whose dimension is different each other. The electrode width (w), spacing (l) are 2 μm and cell thickness d is 6 μm in Cell-1 whereas w, $l = 15$ μm and $d = 10$ μm in Cell-2. No surface treatment was performed on a substrate for multidomain BPLCs. For monodomain BPLCs, on the other hand, the inner surface of substrates was spin-coated with polyimide (AL22620+801, JSR Micro Korea) and was thermally cured at 230 °C for 1 h. A unidirectional rubbing process was carefully done afterward by a velvet cloth. The rubbing direction was fixed at 45° to the long-direction of electrodes. The pretilt angle was measured as 5°. The homogeneous mixture of BPLC was infiltrated into the cells at 70 °C and subsequent characterizations were carried out after few cooling cycles.

Characterizations: The BPLC was identified by photomicrographs observed by a POM (Nikon Eclipse, E600 POL). The temperature of the sample was maintained by the temperature controller (Instec, HSC402-STC20U) with cooling rate 0.3 °C min^{-1}. When BP appears, the temperature was fixed and photopolymerization was carried out at 66.3 °C (BPI) by illuminating UV light (10 mW cm^{-2} for 15 min). The phase range of the sample was verified by observing POM images after polymerization. The Bragg reflection spectra were measured by using a UV–vis spectrometer (USB2000+, Ocean Optics), which is set on the POM. Using the reflection mode of POM, we had light illuminated on the samples and reflected light was guided back to the spectrometer while controlling the temperature in the hot stage. The diffraction properties were measured by linearly polarized

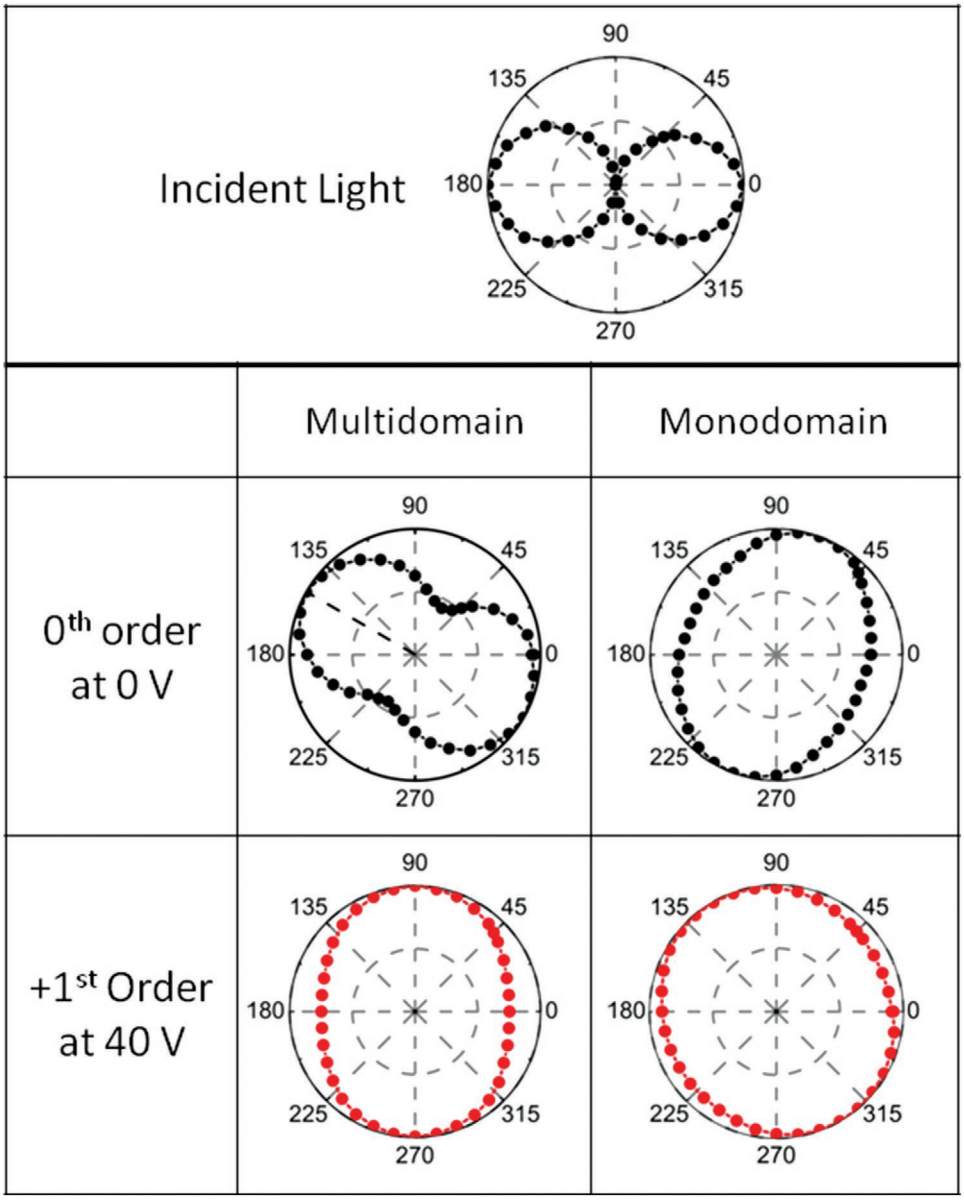

Figure 6. Polarization properties of prepared multidomain and monodomain PS-BPLC at the 0th and 1st orders.

He-Ne laser (633 nm) which is set to incident on the experimental cell and the diffracted light is captured by placing screen behind the cell. The distance between the cell and the screen was fixed to 72 cm. The screen can be replaced by the photodiode connected to digital oscilloscope (Tektronix, DPO2024B) to measure the light energy of the diffracted light. We use TM mode for diffraction measurements. The square-wave voltage with 1 kHz frequency was generated by the function generator (Tektronix, AFG3101C) and modulated by an amplifier (FLC Electronics, A400) is supplied to the cell. Further, the polarization states measurements were performed under crossed polarizers by placing the analyzer behind the cell and voltage-dependent transmission is measured by rotating the analyzer in anti-clock direction. Next, electro-optics such as the response time and switching behavior was studied. Finally, the retardation is measured with REMS-150 (SESIM Photonics Technology, South Korea) for both samples and the bulk images of the cell are also recorded.

Supporting Information

Supporting Information is available from the Wiley Online Library or from the author.

Acknowledgements

This research was supported by the Basic Science Research Program through the National Research Foundation of Korea (NRF) funded by the Ministry of Education (2016R1D1A1B01007189) and by the National Research Foundation of Korea (NRF) grant funded the Korea government (MSIT) (No. 2019R1A5A8080326).

Conflict of Interest

The authors declare no conflict of interest.

Keywords

blue phase liquid crystals, diffraction grating, liquid crystals, monodomain

Received: November 14, 2019
Revised: February 11, 2020
Published online:

[1] H. Coles, S. Morris, *Nat. Photonics* **2010**, *4*, 676.
[2] Y. H. Lin, Y. J. Wang, V. Reshetnyak, *Liq. Cryst. Rev.* **2017**, *5*, 111.
[3] F. Castles, S. M. Morris, J. M. Hung, M. M. Qasim, A. D. Wright, S. Nosheen, S. S. Choi, B. I. Outram, S. J. Elston, C. Burgess, L. Hill, *Nat. Mater.* **2014**, *13*, 817.
[4] H. Lee, H. Park, O. Kwon, S. J. Yun, J. H. Park, S. Hong, S. Shin, *SID Symp. Dig. Tech. Papers* **2011**, *42*, 121.
[5] S. S. Gandhi, M. S. Kim, J.-Y. Hwang, L.-C. Chien, *Adv. Mater.* **2016**, *28*, 8998.
[6] H. Kikuchi, M. Yokota, Y. Hisakado, H. Yang, T. Kajiyama, *Nat. Mater.* **2002**, *1*, 64.
[7] F. Castles, F. V. Day, S. M. Morris, D. H. Ko, D. J. Gardiner, M. M. Qasim, S. Nosheen, P. J. Hands, S. S. Choi, R. H. Friend, H. J. Coles, *Nat. Mater.* **2012**, *11*, 599.
[8] W. He, G. Pan, Z. Yang, D. Zhao, G. Niu, W. Huang, X. Yuan, J. Guo, H. Cao, H. Yang, *Adv. Mater.* **2009**, *21*, 2050.
[9] P. Lin, Z. Wei, Q. Yan, Y. Chen, M. Wu, J. Xie, M. Zeng, W. Wang, J. Xu, Z. Cheng, *J. Mater. Chem. C* **2019**, *7*, 4822.
[10] P. Lin, Q. Yan, Z. Wei, Y. Chen, F. Chen, Z. Huang, X. Li, H. Wang, X. Wang, Z. Cheng, *Opt. Express* **2018**, *26*, 18310.
[11] Z. Ge, S. Gauza, M. Jiao, H. Xianyu, S. T. Wu, *Appl. Phys. Lett.* **2009**, *94*, 101104.
[12] S. Yokoyama, S. Mashiko, H. Kikuchi, K. Uchida, T. Nagamura, *Adv. Mater.* **2006**, *18*, 48.
[13] L. Wang, W. He, X. Xiao, M. Wang, M. Wang, P. Yang, Z. Zhou, H. Yang, H. Yu, Y. Lu, *J. Mater. Chem.* **2012**, *22*, 19629.
[14] K. M. Ge Chen, S. Gauza, H. Xianyu, S. T. Wu, *J. Disp. Technol.* **2010**, *6*, 49.
[15] J. Yan, Y. Li, S. T. Wu, *Opt. Lett.* **2011**, *36*, 1404.
[16] S. J. Ge, W. Ji, G. X. Cui, B. Y. Wei, W. Hu, Y. Q. Lu, *Opt. Mater. Express* **2014**, *4*, 2535.
[17] Y. H. Chen, C. T. Wang, C. P. Yu, T. H. Lin, *Opt. Express* **2011**, *19*, 25441.
[18] C. T. Wang, Y. C. Li, J. H. Yu, C. Y. Wang, C. W. Tseng, H. C. Jau, Y. J. Chen, T. H. Lin, *Opt. Express* **2014**, *22*, 17776.
[19] H. Y. Chen, H. Y. Tu, *OSA Continuum* **2019**, *2*, 478.
[20] M. Wang, C. Zou, J. Sun, L. Zhang, L. Wang, J. Xiao, F. Li, P. Song, H. Yang, *Adv. Funct. Mater.* **2017**, *27*, 1702261.
[21] H. Y. Lin, N. Avci, S. J. Hwang, *Liq. Cryst.* **2019**, *46*, 1359.
[22] Y. T. Lin, H. C. Jau, T. H. Lin, *J. Appl. Phys.* **2013**, *113*, 063103.
[23] L. Gao, Z. Z. Zheng, J. L. Zhu, W. M. Han, Y. B. Sun, *Opt. Lett.* **2016**, *41*, 3775.
[24] Y. Yuan, Y. Li, C. P. Chen, S. Liu, N. Rong, W. Li, X. Li, P. Zhou, J. Lu, R. Liu, Y. Su, *Opt. Express* **2015**, *23*, 20007.
[25] J. L. Zhu, J. G. Lu, J. Qiang, E. W. Zhong, Z. C. Ye, Z. He, X. Guo, C. Y. Dong, Y. Su, H. P. Shieh, *J. Appl. Phys.* **2012**, *111*, 033101.
[26] J. Yan, M. Jiao, L. Rao, S. T. Wu, *Opt. Express* **2010**, *18*, 11450.
[27] R. S. Zola, H. K. Bisoyi, H. Wang, A. M. Urbas, T. J. Bunning, Q. Li, *Adv. Mater.* **2019**, *31*, 1806172.
[28] H. S. Kitzerow, *Mol. Cryst. Liq. Cryst.* **1991**, *202*, 51.
[29] M. S. Kim, L. C. Chien, *Soft Matter* **2015**, *11*, 8013.
[30] E. Oton, E. Netter, T. Nakano, F. Inoue, *Sci. Rep.* **2017**, *7*, 44575.
[31] P. Nayek, H. Jeong, H. R. Park, S. W. Kang, S. H. Lee, H. S. Park, H. J. Lee, H. S. Kim, *Appl. Phys. Express* **2012**, *5*, 051701.
[32] W.-H. Li, D.-C. Hu, Y. Li, C. P. Chen, Y.-J. Lee, A. Lien, J.-G. Lu, Y. Su, *Appl. Phys. Lett.* **2015**, *107*, 241105.
[33] K. Kim, S. Kim, S. Y. Jo, S. W. Choi, *J. Inf. Disp.* **2015**, *16*, 155.
[34] M. R. Wilson, D. J. Earl, *J. Mater. Chem.* **2001**, *11*, 2672.
[35] T. Kato, *Liquid Crystalline Functional Assemblies and Their Supramolecular Structures*, Springer, New York **2001**, pp 99–117.
[36] X. Li, J. A. Martínez-González, J. P. Hernández-Ortiz, A. Ramírez-Hernández, Y. Zhou, M. Sadati, R. Zhang, P. F. Nealey, J. J. de Pablo, *Proc. Natl. Acad. Sci. USA* **2017**, *114*, 10011.
[37] L. Menez, I. Zaquine, A. Maruani, R. Frey, *J. Opt. Soc. Am. B* **2002**, *19*, 965.
[38] J. Yan, H. C. Cheng, S. Gauza, Y. Li, M. Jiao, L. Rao, S. T. Wu, *Appl. Phys. Lett.* **2010**, *96*, 071105.
[39] S. Pagidi, R. Manda, S. S. Bhattacharyya, S. G. Lee, S. M. Song, Y. J. Lim, J. H. Lee, S. H. Lee, *Adv. Mater. Interfaces* **2019**, *6*, 1900841.
[40] M. G. Moharam, L. Young L, *Appl. Opt.* **1978**, *17*, 1757.
[41] W. A. Shurcliff, *Polarized Light: Production and Use*, Harvard University Press, Cambridge, MA **1966**, p. c1966.

